Energy Proceedings
Vol 39, 2024
ISSN 2004-2965

Study on Engineering Parameters and Risks of CO_2 Geological Storage Based on WR-THM Coupling Model

Xinyuan Gao[1], Shenglai Yang[1*], Jiatong Wang[1], Lerao Tian[1], Lufei Bi[1], Haiwei Zuo[1], Bin Shen[1,2*]

1 National Key Laboratory of Petroleum Resources and Engineering, China University of Petroleum (Beijing), 102249, Beijing, China

2 College of artificial intelligence, China University of Petroleum (Beijing), 102249 Beijing, China
(*Corresponding Author: yangsl@cup.edu.cn, binshen0803@163.com)

ABSTRACT

Injecting CO_2 into geological formations can effectively slow down CO_2 emissions. However, during the injection process, the physical properties of CO_2 in the wellbore and reservoir change significantly, which will greatly affect the CO_2 geological storage effect, and even cause injection difficulties or leakage, and the risk of hydrate formation. Therefore, a wellbore-reservoir-thermo-hydro-mechanical (WR-THM) fully coupled model is established. The model considers the heat transfer between the wellbore and the surrounding formation, the coupling between the wellbore and the target reservoir, and the THM coupling process of various fluids in the reservoir. The CO_2 storage effect and possible risks under different engineering parameters were studied. The research results show that when the injection temperature is -10°C, there is a risk of hydrate formation at the bottom hole. Increasing the injected mass flow will greatly reduce the CO_2 injection capacity. Low-permeability reservoirs are not easy to inject, and CO_2 seeps uncontrollably into cap rock and base rock. The research results provide theoretical support for the safe and efficient geological storage of CO_2.

Keywords: CO_2 storage, CCUS, wellbore fluid flow and heat transfer, multiphase flow and heat transfer in porous media, numerical simulation

1. INTRODUCTION

Carbon Capture, Utilization and Storage (CCUS) is a technical means that can effectively slow down global warming [1]. Among them, injecting CO_2 into geological structures for storage is an important step in realizing CCUS. The main scenarios for CO_2 geological storage include unconventional oil and gas reservoirs [2], depleted oil and gas reservoirs, saline aquifers [3], geothermal reservoirs [4], etc. At present, there have been a lot of researches on the geological storage of CO_2. However, the physical properties of CO_2 in the wellbore and reservoir change significantly, which will greatly affect the effect of CO_2 geological storage, and even cause problems of difficulty in injection or the risk of leakage and hydrate formation.

Based on MATLAB Reservoir Simulation Toolbox (MRST), Zhang et al. [5] proved that CO_2 huff 'n' puff is an effective technology for CO_2 storage and enhanced natural gas recovery, but they did not consider the influence of the flow of CO_2 in the wellbore on the physical properties of CO_2 after entering the reservoir. Lei et al. [3] established a wellbore-reservoir coupling model based on the wellbore model CO2WELL and the reservoir simulator TOUGH2\ ECO2N, but the coupling mode is partial coupling, and large errors will occur when CO_2 flows from the wellbore into the reservoir.

Therefore, based on the COMSOL Multiphysics finite element numerical simulation software, this paper establishes a fully coupled wellbore-reservoir-thermo-hydro-mechanical (WR-THM) model. This model considers the heat transfer between the wellbore and the surrounding formation, the coupling between the wellbore and the target reservoir, and the THM of various fluids in the reservoir. Coupling process. The CO_2 storage effect and possible risks under different engineering parameters were studied. The research results provide theoretical support for the safe and efficient geological storage of CO_2.

2. WR-THM MODEL DESCRIPTION

2.1 Physical model and model assumption

The physical model is shown in Fig. 1. The injection well is 2000m deep. Considering that the injection of low-temperature CO_2 will cause significant heat exchange between the wellbore and the surrounding formation, a formation with a radius of 50m is established around it.

This is a paper for 15th International Conference on Applied Energy (ICAE2023), Dec. 3-7, 2023, Doha, Qatar.

Assuming that the caprock, reservoir, and bedrock are all 50m thick, and the radius is 5000m to approximate the infinite boundary.

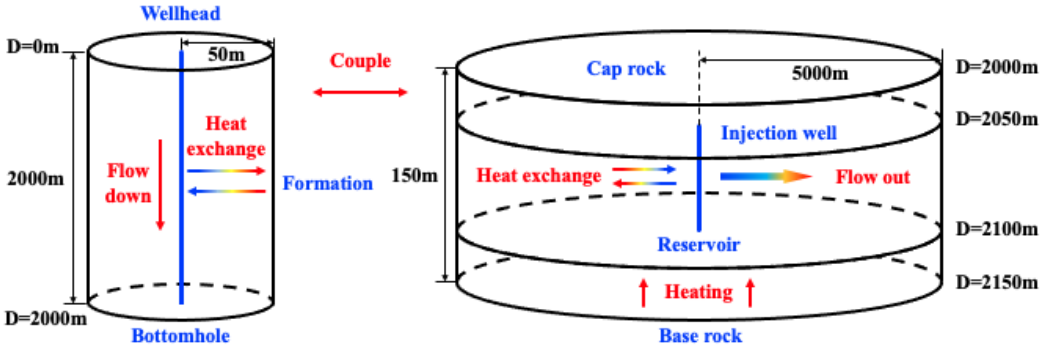

Fig. 1. Physical model

Assuming that the flow of CO_2 and water in the reservoir follows Darcy's law, the injection time is limited to 5 years so chemical reactions are not considered, and the physical properties of CO_2 and water use the data in the NIST database [6].

2.2 Mathematical equations

2.2.1 Wellbore model

The mass, momentum, and energy conservation equations of CO_2 in the wellbore can be expressed as:

$$\frac{\partial A\rho_c}{\partial t}+\nabla\cdot\left(A\rho_c u\right)=0 \tag{1}$$

$$\rho_c\frac{\partial u}{\partial t}+\rho_c u\cdot\nabla u=-\nabla p_w-f_D\frac{\rho_c}{2d_p}u|u|+\rho_c g\sin\vartheta \tag{2}$$

$$\rho_c Ac_{p,c}\frac{\partial T_w}{\partial t}+\rho_c Ac_{p,c}u\cdot\nabla T_w=\nabla\cdot A\lambda_c\nabla T_w+f_D\frac{\rho_c A}{2d_p}|u|^3 -\frac{T_w A}{\rho_c}\left(\frac{\partial\rho_c}{\partial T_w}\right)\left(\frac{\partial\rho_c}{\partial t}+u\cdot\nabla p_w\right)+Q \tag{3}$$

Where ρ_c (kg/m^3) is the fluid density and A (m^2) is tubing cross-sectional area. u (m/s) is fluid velocity. p_w (Pa) and d_p (m) represent the pressure and the diameter of the pipe. f_D is the friction coefficient. $c_{p,c}$ (J/(kg·℃)) and T_w (℃) are the fluid thermal capacity and temperature. λ_c (W/(m·℃)) denotes CO_2 heat conductivity. The third term on the right of Eq. (3) denotes pressure work. Q (w/m) is the heat exchange between wellbore and formation.

The energy conservation equation in the formation can be calculate expressed as:

$$\rho_r c_p\frac{\partial T}{\partial t}+\rho_r c_{p,r}u\cdot\nabla T-\nabla\cdot\left(\lambda_r\nabla T\right)=q_e \tag{4}$$

Where ρ_r (kg/m^3) and $c_{p,r}$ (J/(kg·℃)) represent the density and thermal capacity of the formation.

2.2.2 Reservoir model

The gas-water two-phase flow in the reservoir can be expressed as:

$$\frac{\partial}{\partial t}\left(\varphi\rho_\alpha s_\alpha\right)+\nabla\cdot\left(\rho_\alpha u_\alpha\right)=q_\alpha \tag{5}$$

$$u_\alpha=-\frac{k_\alpha k}{\mu_\alpha}\left(\nabla p_\alpha-\rho_\alpha g\nabla z\right) \tag{6}$$

Where α stands for CO_2 or formation water. φ and k (m^2) are the porosity and permeability of the reservoir. ρ_α (kg/m^3), s_α, u_α (m/s), p_α (Pa), k_α (m^2) and μ_α (Pa·s) are density, saturation, relative permeability and viscosity of fluids.

Changes in temperature and pore pressure both lead to changes in the effective stress of the rock [7]:

$$\Delta\sigma'_m=\alpha\left(P-P_{ini}\right)-3\beta K_B\left(T-T_{ini}\right) \tag{7}$$

Where σ'_m (Pa) is the effective stress. α represent the Biot's coefficient. β (1/℃) is the thermal expansion coefficient and K_B (Pa) is the bulk modulus. P_{ini} (Pa) and T_{ini} (℃) are the initial temperature and pressure.

The change of porosity and permeability [8] can be expressed as:

$$\varphi=\varphi_r+\left(\varphi_0-\varphi_r\right)^{a\Delta\sigma'_m} \tag{8}$$

$$K=K_0\left(\frac{1-\varphi_0}{1-\varphi}\right)^2\left(\frac{\varphi}{\varphi_0}\right)^3 \tag{9}$$

Where φ_0 and K_0 (m^2) are the porosity and permeability when the stress is 0. φ_r is the porosity achievable under stress. a indicates the stress coefficient.

The energy conservation equation of the reservoir and the fluid in the reservoir can be calculated as:

$$\left(\rho c_{\mathrm{p}}\right)_{\mathrm{eff}} \frac{\partial T}{\partial t}+\rho_{\mathrm{f}} c_{\mathrm{p,f}} u_{\mathrm{f}} \cdot \nabla T-\nabla \cdot\left(\lambda_{\mathrm{eff}} \nabla T\right)=q_{\mathrm{e}} \tag{10}$$

2.2.3 Coupling method

By setting the bottom hole pressure to be equal to the reservoir injection pressure, the reservoir injection mass flow rate to be equal to the bottom hole mass flow rate, and the reservoir injection temperature to be equal to the bottom hole temperature to realize the coupling between the wellbore and the reservoir. Realize THM coupling through the simultaneous connection between equations (1)-(10).

3. RESULTS AND DISCUSSIONS

3.1 CO_2 geological storage case

The parameters required for wellbore and reservoir calculations are shown in Tables 1 and 2. The reservoir pressure and temperature gradient are set to 9800Pa/m and 28°C/km, respectively. Assume that under the initial conditions, the wellhead is injected at a constant mass flow rate of 5 kg/s, and the injection temperature is 0 °C.

Table 1 Parameters of wellbore zone model.

Diameter (m)	Values	Thermal conductivity (W/(m·°C))	Values
Tubing inner diameter d_1	0.062	Tubing λ_1	44.7
Tubing outer diameter d_2	0.073	Annulus λ_2	0.56
Casing inner diameter d_3	0.124	Casing λ_3	44.7
Casing outer diameter d_4	0.137	Cement λ_4	0.63
Cement outer diameter d_5	0.216	Formation	2.5

Table 2 Parameters of reservoir zone model.

Parameters	Cap rock	Reservoir	Base rock
Density (kg/m^3)	2600	2300	2600
Thermal conductivity (W/(m·°C))	2.5	2.5	2.5
Thermal capacity (J/(m^3·°C))	850	900	850
Zero-stress porosity (%)	5	15	5
Residual porosity (%)	5	2	5
Permeability (mD)	0.05	30	0.05
Linear thermal-expansion coefficient (1/°C)	10^{-6}	10^{-6}	10^{-6}
Stress coefficient (1/Pa)	2×10^{-8}	2×10^{-8}	2×10^{-8}
Elastic modulus (Pa)	2.5×10^{10}	2.5×10^{10}	2.5×10^{10}
Poisson's ratio	0.25	0.25	0.25
Biot's coefficient	1	1	1

3.2 Analysis of wellbore flow

To study the thermal characteristics of the wellbore model, it is necessary to analyze the temperature field of the wellbore model. The wellbore model simulates the heat exchange between the 1D wellbore and the 3D formation. Fig. 2 depicts the temperature and pressure distribution along the wellbore depth after 5 years of injection assuming a base case, no 3D Formation case, and no pressure work case. It can be observed from the figure that the pressure work of 3D formation and CO_2 in the wellbore model has a noticeable effect on the temperature and pressure distribution of the wellbore. When there is no 3D formation part in the wellbore model, the 1D wellbore will lose the local heat transfer coupling relationship with the 3D formation, and the temperature of the outer wall of the wellbore cannot be reduced, which will lead to the change of the temperature and pressure in the wellbore. When CO_2 pressure work is not considered, the volume change of CO_2 will not do work to the outside, which will lead to the change of temperature and pressure in the wellbore.

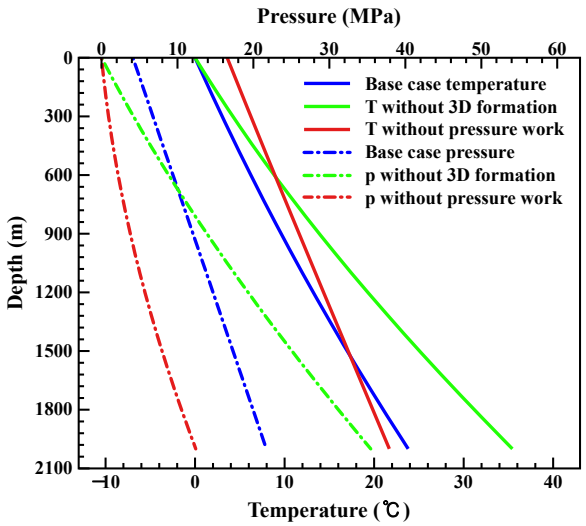

Fig. 2. Temperature and pressure distribution along the wellbore depth after 5 years of injection assuming a base case, no 3D Formation case, and no pressure work case.

3.3 Influence of injection temperature

The injection temperature will significantly affect the physical properties of CO_2, and then affect its storage process. Therefore, the injection temperature range of -10°C-20°C was selected to study its influence. Figure 3 shows the changes in bottom hole temperature (BHT) and wellhead pressure (WHP) over the 5-year period of

injection. As the injection temperature decreases, the BHT will decrease significantly, making CO_2 easier to inject.

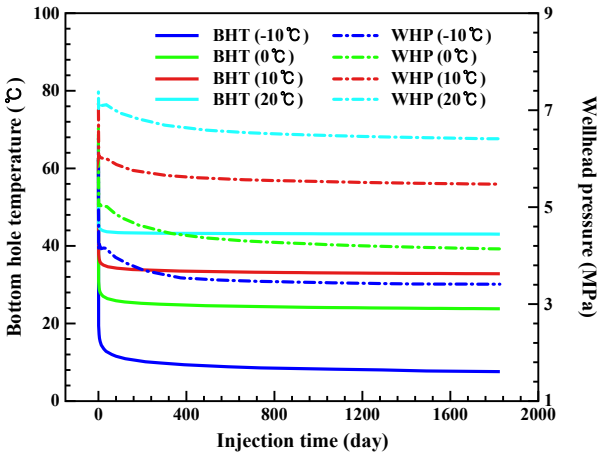

Fig. 3. BHT and WHP under different injection temperature.

Fig. 4 shows the bottom hole pressure (BHP), p-T curves and hydrate formation curves at different injection temperatures. Injection temperature has little effect on BHP. The p-T curve is a relationship curve describing the BHP and BHT, and it is used together with the hydrate formation curve to judge the possible hydrate formation between CO_2 and water at the bottom hole. It can be seen from the figure that with the decrease of BHT, BHP will rise rapidly after a steady rise, and then fall rapidly. As the injection temperature increases, the p-T curve will shrink along the positive x-axis based on the initial point. It is worth noting that when the injection temperature is -10 °C, the p-T curve will intersect with the hydrate formation curve, which means that there is a risk of hydrate formation at the bottom of the well as the injection time increases.

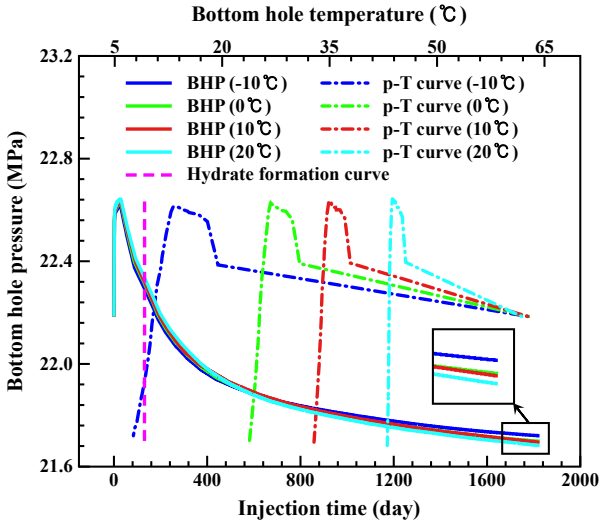

Fig. 4. BHP and p-T curves under different injection temperature and hydrate formation curve.

Fig. 5 depicts the porosity and permeability distribution along the x-axis (y = 0 m, z = -2075 m) under different injection temperature. Obviously, as the injection temperature increases, the variation of porosity and permeability near the bottom hole will decrease. Compared with the injection temperature -10℃, the porosity and permeability decreased by 0.0047 and 3.54mD when the injection temperature was 20℃. It is worth noting that the influence range in the x-axis direction is about 200m, and the influence range is not affected by the injection temperature.

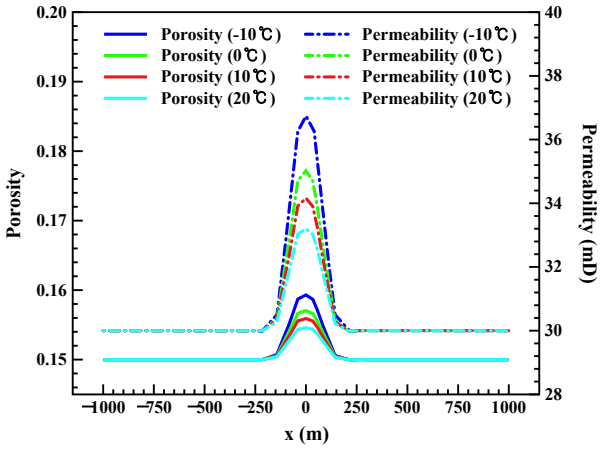

Fig. 5. Porosity and permeability distribution under different injection temperature.

3.4 Influence of injection mass flow

The injection mass flow rate will directly affect the speed and injection capacity of CO_2 storage into the reservoir, so the injection mass flow rate range of 2.5-10kg/s is selected to study its influence. Figure 6 shows the BHT and WHP at different injected mass flow rates. The increase of injected mass flow rate will weaken the BHT reduction but will significantly increase the WHP.

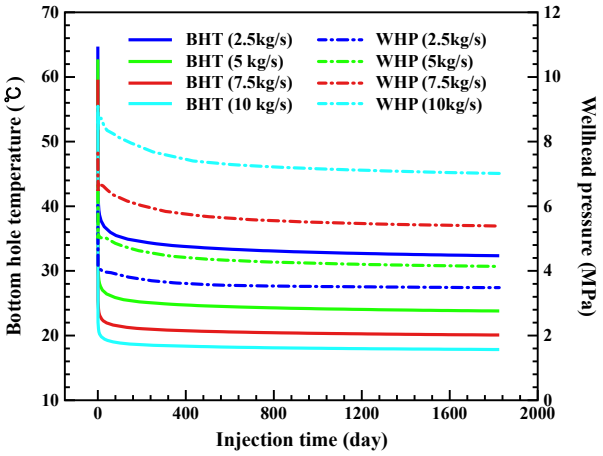

Fig. 6. BHP and WHP under different injection mass flow.

Fig. 7 shows the BHP, p-T curves, and hydrate formation curve at different injection mass flow rates. Apparently, the changes of BHP and p-T curves are consistent with those in Figure 4. The difference is that the BHP increases substantially as the injected mass flow rate increases. This is because more CO_2 accumulated in the reservoir will significantly increase BHP. After BHP reaches the maximum value, as the injected mass flow rate increases, the time when BHP begins to decrease will be earlier, because the influence range of CO_2 will expand with the increased injected mass flow rate. For the p-T curve, the higher injected mass flow rate p-T curve will not intersect the hydrate curve. Therefore, although there is no risk of hydrate formation in large flow rates, it will lead to an increase in reservoir pressure, thereby reducing injection capacity.

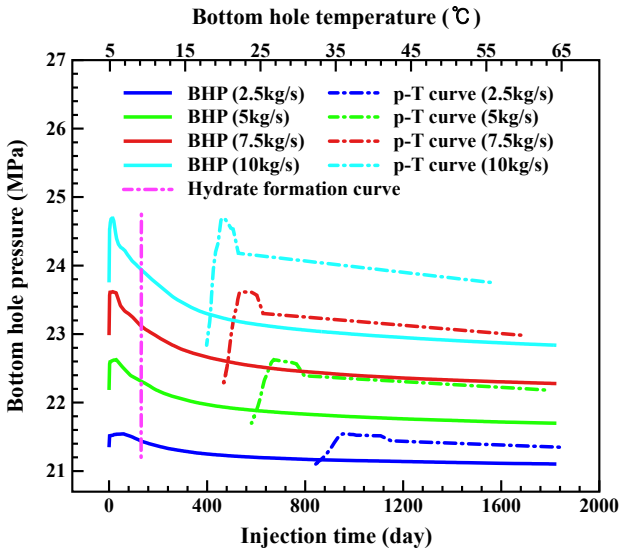

Fig. 7. BHT and p-T curve under different injection mass flow.

Fig. 8 depicts the distribution of porosity and permeability along x at different injected mass flow rate. Different from Fig. 5, the influence range of the low temperature region is also affected by the injection mass flow rate. With the increase of injected mass flow rate, the influence area expanded from 143.24m to 270.09m. Therefore, a higher injection mass flow rate should be used to improve the porosity and permeability of the reservoir near the bottom hole and their variation range.

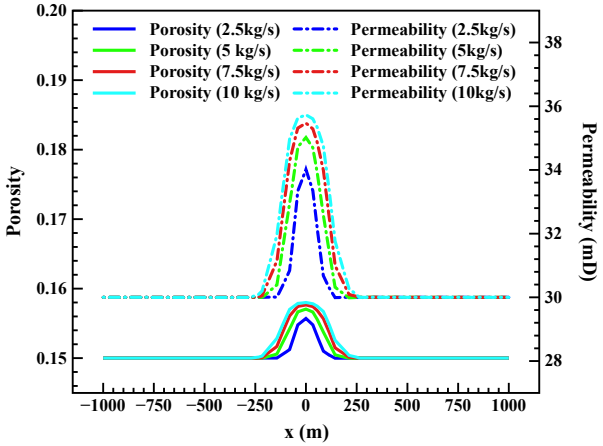

Fig. 8. Porosity and permeability distribution under different injection mass flow.

3.5 Influence of reservoir porosity

Fig. 9 illustrates WHP and BHP curve under different reservoir porosity ϕ0 (0.1, 0.15, 0.2, 0.25). It can be observed from the figure that WHP and BHP are less affected by porosity. With the increase of porosity, WHP and BHP show a slight increase trend. Among them, the maximum difference between WHP and BHP under different porosity is 0.11MPa and 0.12MPa. This is because higher porosity will reduce the sweep scope of CO_2, resulting in CO_2 accumulation near the bottom hole.

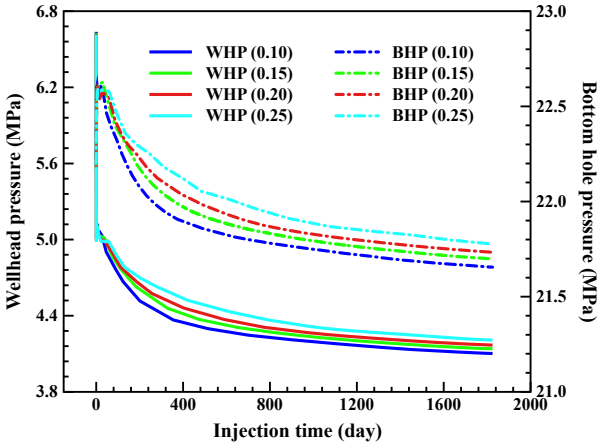

Fig. 9. WHP and BHP curve under different reservoir porosity φ_0.

Fig. 10 depicts the CO_2 sweep scope in the reservoir and breakthrough distance in the cap rock under different reservoir porosity. Obviously, the CO_2 sweep scope in the reservoir under different porosity exceeds 400m, and the maximum is close to 700m. With the increase of porosity, the sweep scope of CO_2 in the reservoir gradually decreases. This is because higher porosity means more storage space for CO_2, so it is impossible to make CO_2 have a wider sweep scope. The breakthrough distance of CO_2 in

the cap rock is less affected by the porosity, which is within the range of 14-15m. The breakthrough distance decreases slightly with the increase of porosity.

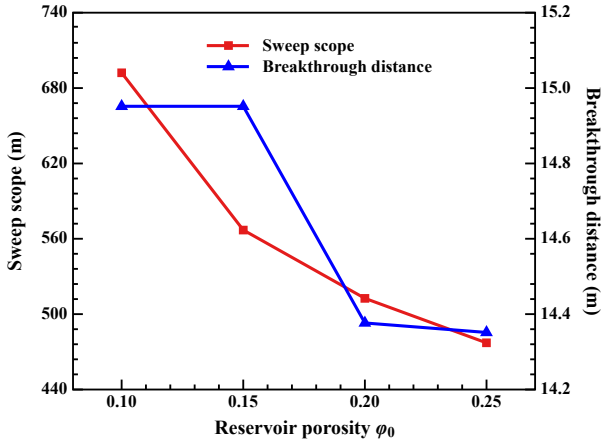

Fig. 10. CO_2 sweep range in the reservoir and breakthrough distance in the cap rock under different reservoir porosity φ_0.

Fig. 11 shows the CO_2 storage efficiency in reservoir, cap rock, and base rock under different reservoir porosity. It can be observed from the figure that with the increase of porosity, the CO_2 storage efficiency in the reservoir, cap rock and base rock will decrease significantly. It is worth noting that compared with the equivalent porosity (linear expansion the storage efficiency when the porosity is 0.1), the actual CO_2 storage efficiency in the reservoir is slightly higher, but the storage efficiency in the cap rock and base rock is markedly reduced. This is because the breakthrough distance of CO_2 in the cap rock and base rock will decrease with the increase of porosity. Based on the above-mentioned analysis, porosity has little effect on CO_2 flow and heat transfer. Higher reservoir porosity can obtain a higher CO_2 storage capacity and less CO_2 leakage. Therefore, to obtain higher CO_2 storage effect, reservoirs with higher porosity should be selected as much as possible.

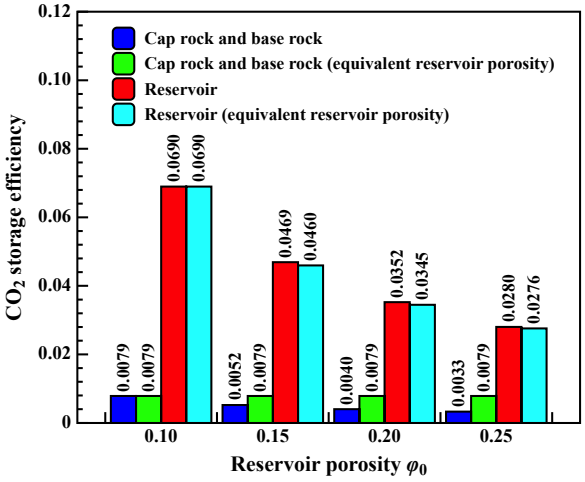

Fig. 11. CO_2 storage efficiency in reservoir, cap rock, and base rock under different reservoir porosity φ_0.

3.6 *Influence of reservoir permeability*

Fig. 12 shows WHP and BHP curves under different reservoir permeability K_0 (10mD, 30mD, 50mD, 100mD). WHP and BHP show a decreasing trend with the increase of permeability. It is worth noting that when the permeability is 10mD, WHP and BHP will be greatly increased. Among them, the WHP and BHP difference at the permeability of 10mD and 30mD are 2.36MPa and 2.70MPa. Indicating that lower permeability will give more resistance to CO_2 injected into the reservoir.

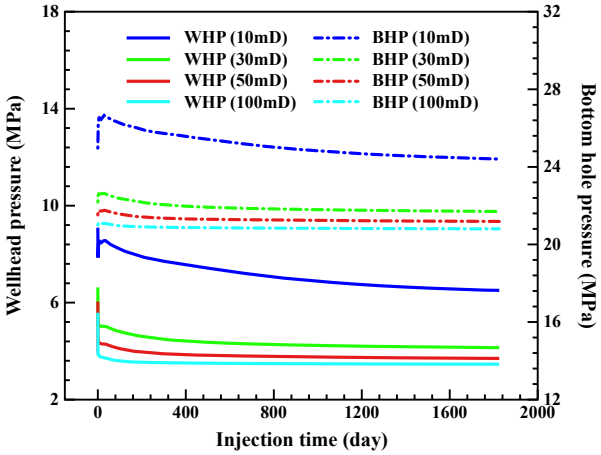

Fig. 12. WHP and BHP curve under different reservoir permeability K_0.

Fig. 13 depicts the CO_2 sweep range in the reservoir and breakthrough distance in the cap rock under different reservoir permeability. Obviously, the CO_2 sweep scope in the reservoir under different permeability exceeds 400m, and the maximum is close to 700m. With the increase of permeability, the sweep scope of CO_2 in the reservoir gradually increases. This is because higher permeability means that CO_2 has better flow capacity in the reservoir.

The breakthrough distance of CO_2 in the cap rock is less affected by the permeability when the permeability is 30-100mD. At this time, the breakthrough distance of CO_2 in the cap rock increases slowly with the decrease of permeability. It is worth noting that when the permeability is reduced to 10mD, the breakthrough distance of CO_2 in the cap rock will be greatly increased to nearly 20m. This is because when the permeability of the reservoir is low, the permeability of the reservoir is close to that of the cap rock. At this time, a large amount of CO_2 will flow into the cap rock and base rock.

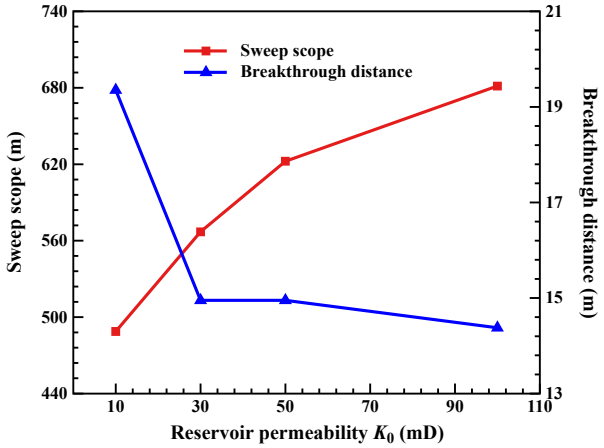

Fig. 13. CO_2 sweep range in the reservoir and breakthrough distance in the cap rock under different reservoir permeability K_0.

Fig. 14 shows the CO_2 storage efficiency in reservoir, cap rock, and base rock under different reservoir permeability. It can be observed from the figure that the CO_2 storage efficiency in the reservoir, cap rock, and base rock will increase slightly with the increase of permeability. This is because with the increase of permeability, the decrease of BHP will lead to a decrease in CO_2 density, resulting in a larger volume of CO_2. At the same time, with the increase of permeability, although the breakthrough distance of CO_2 in the cap rock gradually decreases, the sweep range of CO_2 in the reservoir is wider, which means that the breakthrough area of CO_2 is wider. Based on the above-mentioned analysis, larger permeability is conducive to CO_2 injection while reducing CO_2 leakage to the cap rock and base rock.

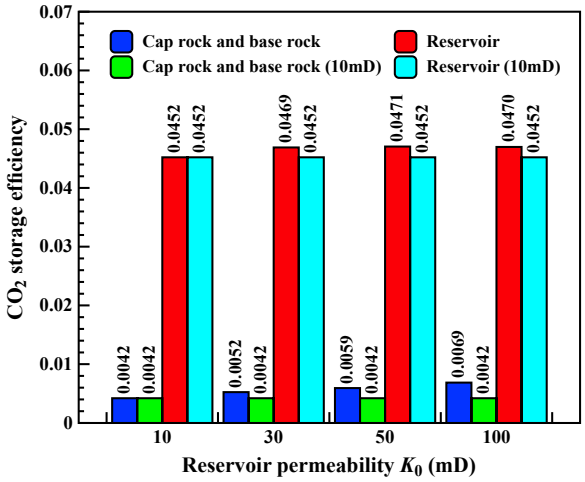

Fig. 14. CO_2 storage efficiency in reservoir, cap rock, and base rock under different reservoir permeability K_0.

4. CONCLUSIONS

The main conclusions are as follows:

(1) The 3D formation and the CO_2 pressure work are highly significant to the temperature and pressure distribution in the wellbore.

(2) Lower injection temperature will result in higher injection capacity and lower pore volume occupancy. However, there is a risk of hydrate formation near the bottom hole. A higher injection mass flow rate can achieve greater CO_2 storage efficiency without the risk of hydrate formation but will weaken the injection capacity of CO_2. Simultaneously, the alteration of injection parameters will change the porosity and permeability of the reservoir near the bottom hole, and then affect the CO_2 injection capacity and storage capacity.

(3) The porosity and permeability of the reservoir are key factors affecting the CO_2 storage effect. Porosity has little effect on the non-isothermal flow of CO_2. Bigger porosity can obtain better CO_2 storage capacity. Larger permeability is conducive to CO_2 injection while reducing CO_2 leakage to the cap rock and base rock.

ACKNOWLEDGMENT

The authors would like to acknowledge the National Natural Science Foundation of China (51774300) and National Science and Technology Major Project (2016ZX05016-006-004) for their financial support.

DECLARATION OF INTEREST STATEMENT

The authors declare that they have no known competing financial interests or personal relationships that could have appeared to influence the work reported in this paper. All authors read and approved the final manuscript.

REFERENCE

[1] Al Baroudi, H., Awoyomi, A., Patchigolla, K., Jonnalagadda, K., & Anthony, E. J. (2021). A review of large-scale CO2 shipping and marine emissions management for carbon capture, utilisation and storage. Applied Energy, 287, 116510.

[2] Liu, X., Sang, S., Zhou, X., & Wang, Z. (2023). Coupled adsorption-hydro-thermo-mechanical-chemical modeling for CO2 sequestration and well production during CO2-ECBM. Energy, 262, 125306.

[3] Lei, H., Cai, Y., Lu, M., Li, X., & Connell, L. D. (2020). A study on the thermal-hydrodynamical-coupled CO2 flow process in the Ordos CCS-geological-formation. International journal of greenhouse gas control, 95, 102999.

[4] Shi, Y., Song, X., Wang, G., McLennan, J., Forbes, B., Li, X., & Li, J. (2019). Study on wellbore fluid flow and heat transfer of a multilateral-well CO2 enhanced geothermal system. Applied energy, 249, 14-27.

[5] Zhang, R. H., Wu, J. F., Zhao, Y. L., He, X., & Wang, R. H. (2021). Numerical simulation of the feasibility of supercritical CO2 storage and enhanced shale gas recovery considering complex fracture networks. Journal of Petroleum Science and Engineering, 204, 108671.

[6] Linstrom, P. J., & Mallard, W. G. (2001). The NIST Chemistry WebBook: A chemical data resource on the internet. Journal of Chemical & Engineering Data, 46(5), 1059-1063.

[7] McTigue, D. F. (1986). Thermoelastic response of fluid-saturated porous rock. Journal of Geophysical Research: Solid Earth, 91(B9), 9533-9542.

[8] Han, X., Feng, F., Yan, M., Cong, Z., Liu, S., & Zhang, Y. (2022). CO2–water–rock reaction transport via simulation study of nanoparticles-CO2 flooding and storage. Sustainable Energy Technologies and Assessments, 50, 101736.